A high-resolution 3D emissions inventory of airport and its hotspot detection: A case study of Beijing Capital International Airport, China

Zhoushun Han [a,b], Hengcai Zhang [a,c,*] , Jinzi Wang [a,c], Xin Fu [b], Peixiao Wang [a,c] ,
Jianing Yu [a,c] , Yafei Li [d]

[a] State Key Laboratory of Resources and Environmental Information System, Institute of Geographic Sciences and Natural Resources Research, Chinese Academy of Sciences, Beijing, 100101, China
[b] School of Water Conservancy and Environment, University of Jinan, 250022, Shandong, China
[c] College of Resources and Environment, University of Chinese Academy of Sciences, Beijing, 100049, China
[d] College of Air Traffic Management, Civil Aviation University of China, Tianjin, 300300, China

A R T I C L E   I N F O

A B S T R A C T

Airports, as significant sources of greenhouse gas emissions, play a crucial role in mitigating global climate warming. Existing studies mainly focus on the specific emission values of airports and lack effective methods to calculate high-resolution 3D emissions inventories. To address this gap, we propose a 3D High Emission Estimation method (3D-HEE) to estimate the high-dimensional emissions of airports, including carbon dioxide (CO_2), carbon monoxide (CO), hydrocarbons (HC), and nitrogen oxides (NO_x). We firstly calculate the emission points of the single aircraft trajectory. All emission points within the airport region are aggregated, and we develop an improved Three-dimensional empirical Bayesian kriging (3D-EBK) to estimate airport's 3D emissions inventory. Secondly, we introduce a novel Local Emission Peak Indicator (LEPI) and propose a hotspot detection algorithm to identify irregular high emission areas in a 3D emissions inventory. Applied to Beijing Capital International Airport (PEK), our method identified three CO_2 hotspots (HEIH1-3) near Terminal 1, the Capital Airport Line, and taxiways, confined to heights of 0–37.18 m due to CO_2 diffusion patterns. CO and HC hotspots (HEIH1-2) clustered at 40.06°N–40.08°N, 116.58°E−116.61°E and runway starts (0–37.18 m), suggesting shared emission mechanisms. In contrast, NO_x hotspots spanned altitudes from ground level to 889.04 m, with HEIH1 (389.03–889.04 m) likely linked to climb-phase emissions. The 3D-HEE method precisely resolves emission structures (e.g., flat ellipsoids for CO_2, elevated plumes for NO_x), providing actionable insights for airport-specific decarbonization strategies, such as optimizing ground operations and flight trajectories.

1. Introduction

With the rapid development of civil aviation, the atmospheric pollutants in the exhaust emissions from airport aircraft, including CO_2 CO, NO_x, SO_2, HC, and $PM_{2.5}$, are having an increasingly significant impact on the environment(Mardani et al., 2019; Ouyang and Lin, 2017; Du et al., 2017). As a key location for aircraft takeoffs and landings, airports are often affected by elevated local concentrations of atmospheric pollutants from aircraft emissions in the surrounding environment(Xiong et al., 2023; Fung et al., 2008; Zhang et al., 2019). According to relevant studies, the total emissions of NO_x and CO from airport aircraft account for approximately 4 % of the emissions produced by mobile pollution sources. As a reference for aviation kerosene consumption, for every 1 ton of aviation kerosene consumed, an aircraft typically emits 3187.00 kg of CO_2, 0.98 kg of SO_2, 0.56 kg of CO, and 21.12 kg of NO_x(Wang et al., 2023; Klapmeyer and Marr, 2012; Monsalud et al., 2015; Bastress, 1973; Hu et al., 2020).

Currently, airports face a dual dilemma of excessive carbon emissions and low operational efficiency during their operations(Zhang et al., 2019; Klapmeyer and Marr, 2012). Traditional airport operating models often focus on meeting basic flight takeoff and landing needs as well as passenger service demands, while neglecting the optimization of energy utilization efficiency and carbon emissions. The various complex facilities, equipment, and diverse operational processes within the

---

airport are intertwined, leading to uneven energy consumption distribution and significant waste, making it difficult to enhance the overall operational efficiency of airports, and exacerbating the carbon emissions issue(Klapmeyer and Marr, 2012; Ashok et al., 2017; Kılkış, 2014; Kelemen et al., 2020). In addition to emissions from aircraft operations, airport terminal buildings also contribute significantly to energy consumption and CO_2 emissions, particularly through HVAC systems in extreme climates(Yildiz et al., 2022).

Current research on aviation emissions is relatively mature, with various calculation methods and models established, such as the International Civil Aviation Organization (ICAO) calculation method (Mackenzie, 2010) and the Sabre Holdings method, which provide tools for quantifying aviation emissions (Yaohui et al., 2023; Graver and Frey, 2009). Research on aviation emissions mainly focuses on the quantitative assessment and measurement of aviation emissions, the impact of aviation emissions on the environment and climate, reduction paths and technological innovations in the aviation industry, and the regional distribution and spatial characteristics of aviation emissions. The assessment of aviation emissions relies on flight data and models to calculate the emissions of gases such as CO_2 and NO_x. This measurement provides a basis for formulating reduction policies. For example, studies indicate that aviation CO_2 emissions account for approximately 2 % of global total emissions(Sun et al., 2022). A study evaluated the air pollutants emitted by civil aircraft at Athens International Airport during takeoff and landing from 2002 to 2019. The pollutants evaluated include carbon dioxide, nitric oxide, carbon monoxide, hydrocarbons and particulate matter. The research results reveal the large-scale emissions of these pollutants during specific periods and suggest that measures should be taken in the future to mitigate their impact on the environment(Christodoulakis et al., 2022). Relevant models further quantify the emission contributions during different flight phases (such as takeoff and cruising). The calculation of aviation emissions is usually based on models, such as the EDGAR global emissions database and the ICAO model, combined with specific flight fuel consumption and flight distance data. Research shows that existing assessment methods can be accurate to the level of aircraft type and flight route, but there is still room for improvement to further enhance spatial and temporal resolution (Ashok, 2011). The impact of aviation emissions on climate mainly manifests in the long-term effects of CO_2 and the short-term effects of non-CO_2 gases (such as NO_x and water vapor) on radiative forcing. Studies indicate that the contribution of non-CO_2 emissions to climate may even exceed the direct effects of CO_2(Lee et al., 2009). In addition, contrails and cirrus clouds formed at high altitudes significantly enhance the greenhouse effect(Takeda et al., 2008). The climate effects of aviation emissions are not limited to CO_2; they also include the impact of NO_x and water vapor on ozone and cirrus cloud formation(Varotsos et al., 2014). Recent studies show that non-CO_2 emissions account for 4.9 % of the radiative forcing caused by aviation emissions, mainly from the contrail effect. Explorations of aviation emission reductions involve new energy technologies (such as hydrogen fuel and electric aircraft), the application of biofuels, and the optimization of flight routes and altitudes to reduce fuel consumption. Technological advancements in the next 20–40 years (such as zero-emission engines and alternative fuels) are expected to significantly reduce emissions, but studies point out that existing technologies are unlikely to fully achieve the reduction targets set by ACARE and NASA, making additional policies and behavioral interventions potentially critical (Graham et al., 2014). Aviation emissions exhibit significant regional characteristics, with high emissions concentrated in the major hub airport areas of economically developed countries. This emission pattern warrants attention for its regional impact on air quality. The analysis of regional aviation emissions reveals a phenomenon of deteriorating air quality around airports, primarily caused by increases in PM2.5 and NO_x concentrations, which significantly impact public health(Masiol and Harrison, 2014a). However, existing research on airport carbon emissions mostly remains at the level of rough estimates of carbon distribution. Previous research

methods mainly relied on macro statistical data and simplified model assumptions, lacking a detailed depiction and in-depth analysis of carbon emission sources within airports. This extensive research approach makes it difficult to accurately capture the actual situation of carbon emissions at airports, and it cannot provide precise decision-making support for energy-saving and emission-reduction measures.

In view of this, it is extremely urgent to carry out high-resolution 3D high emissions inventory and the identification of irregular 3D hotspot. Through accurate 3D scale estimation, a detailed picture of carbon emissions in the 3D space of the airport can be presented in all directions and at multiple levels, providing a sufficient data basis for in-depth exploration of the causes, transmission paths and dynamic change laws of aviation emissions. Irregular 3D hotspot refers to the concentrated area of aviation emissions with unique spatio-temporal distribution characteristics formed by the interweaving and interaction of aircraft operation trajectories, ground traffic flow, energy consumption of various facilities in the terminal building and surrounding environmental factors in the 3D space of the airport. Physically speaking, it represents the aggregation pattern of energy consumption and aviation emissions in the complex system of the airport. The accurate identification of irregular 3D hotspots helps to precisely locate the weak links and potential optimization directions in the airport's operating mechanism, thus providing crucial support for formulating highly targeted energy-saving and emission-reduction strategies, effectively improving the energy utilization efficiency and overall operational benefits of the airport, and vigorously promoting the airport to move forward in a low-carbon, environmentally friendly and sustainable direction.

This study proposes a method for 3D estimation of low-altitude airport emissions and detection of high emission irregular hotspots, called the 3D High Emission Estimation method (3D-HEE). Firstly, aviation emissions of aircraft trajectory points were calculated using TrajEmission method(Wang et al., 2024a). Second, the empirical Bayesian Kriging (EBK) method is used to estimate the aviation emissions points of trajectory, and the points are interpolated as voxel (Gribov and Krivoruchko, 2020). Then, the method calculates the Local Emission Peak Indicator (LEPI) for all voxels based on the neighborhood space. LEPI is a quantitative measure used to determine the degree of emission of a single voxel relative to its neighboring space. Based on the results of the LEPI calculation, a dynamic threshold is selected to identify high-emission voxels. Finally, 3D DBSCAN is utilized to cluster the high-emission voxels into high emission irregular hotspot (HEIH)(Chen et al., 2022). And we utilize 3D-HEE to conduct a detection of 3D high emissions at Beijing Capital International Airport (PEK).

The structure of this paper is as follows: Section II introduces research methods; Section III showcases the data of case study and the results of HEIH detecting; Section IV is the discussion, discussing the causes of method and HEIHs' impact on airport operations; Finally, Section V concludes with a summary of the research findings.

2. Methodology

This study puts forward a detection method for identifying the 3D high emission irregular hotspots. It is named 3D High Emission Estimation method (3D-HEE). It is mainly divided into 3 parts: Emission estimation, 3D space estimation, and Emission hotspot identification. The flow chart of the model is shown in Fig. 1.

2.1. Emission estimation

The first part of the 3D-HEE method uses our previously proposed TrajEmission(Wang et al., 2024b) method to estimate emissions from flight trajectories. It consists of three parts: trajectory interpolation, fuel consumption calculation, and emission calculation. It addresses missing parts in the flight trajectory. Using the open-source toolkit OpenAP(Sun et al., 2020) and its internal kinematic aircraft performance model (WRAP) (Sun et al., 2019), the interpolation method is determined
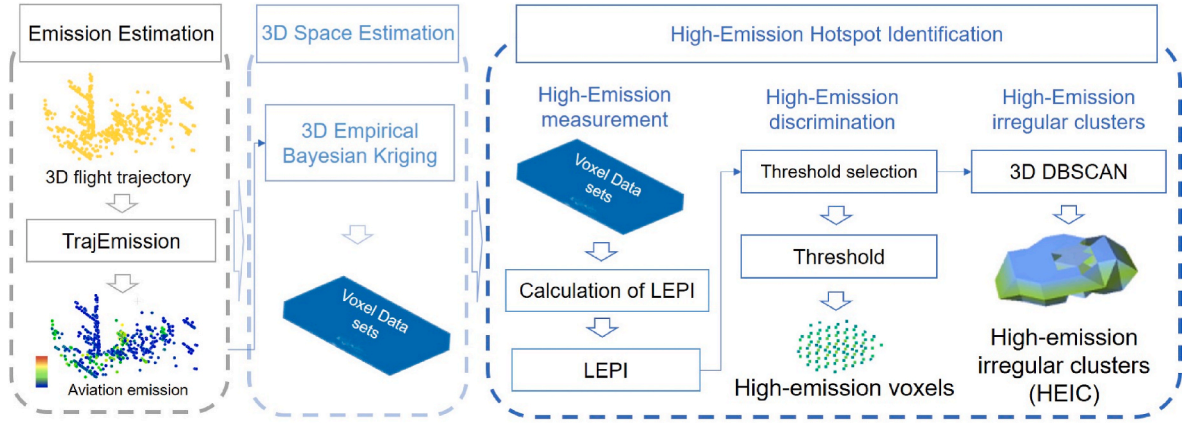
Fig. 1. 3D-HEE algorithm process.

based on the completeness of the flight phase. When there is a discontinuity in the flight trajectory, if the missing parts are minimal, linear regression is first attempted to fill in the missing field values. If there are extensive missing parts or if the flight phase is incomplete (such as missing key climb–cruise–approach phases), the WRAP model is used for simulation interpolation. For fuel consumption calculations, the calculation model from TrajEmission is used. The relationship between fuel consumption and fuel flow is as shown in Equation (1).

$$FC = \sum FF_{fp,eng,alt} \times N_{eng} \times t_{fp} \tag{1}$$

where *FC* denotes the fuel consumption of all phases for a flight. It is the summary result of each flight segment. $FF_{fp,eng,alt}$ represent the fuel flow rate in *fp* during the flight stage. The engine type is *eng* and the height is *alt*. N_{eng} is the engine number of the engine type. The mode time t_{fp} depends on the operating program.

In practical operations, ground speed is used instead of true airspeed, and the default engine type for different aircraft in OpenAP is referenced as the eng parameter. At the same time, considering the impact of aircraft weight on fuel consumption, a method similar to TrajEmission is adopted, selecting 100 %, 70 %, and 50 % of the Maximum Takeoff Weight (MTOW) for comparative analysis. During the calculation process, the aircraft weight is updated in real-time by subtracting the fuel mass consumed during each flight segment. This accurately reflects the impact of the aircraft's weight changes during the flight on fuel consumption, resulting in more precise fuel consumption data. The emission calculation follows the emission model from TrajEmission, i.e., Equation (2):

$$Emiss_{pollu} = \sum FC_i \times EI_{p,i} \tag{2}$$

where $Emiss_{pollu}$ represents the total amount of aviation emissions contaminated by specific pollutants under all flight trajectories.

FC_i represents the fuel consumption of trajectory *i*. $EI_{p,i}$ means the emission indices of pollutant *p* with trajectory *i*.

The Emission Index (EI) quantifies the intensity of pollutant emissions per unit of fuel consumption, with its value influenced by various environmental factors such as temperature, humidity, pressure, and flight conditions (e.g., Mach number, altitude). To achieve a standardized assessment of emission intensity, this study employs a dynamic correction method that maps the atmospheric conditions corresponding to actual flight trajectories to the International Standard Atmosphere (ISA) sea level benchmark. The specific process includes: first, quantifying the deviation between the actual environment and the ISA standard using parameters Mach number correction factor β (Equation (3)), the temperature ratio θ (Equation (4)) the pressure correction parameters δ (Equation (5)) and altitude-related parameter ω (Equation (6)); second, constructing a reference function for fuel flow (FF) and emission

index based on a parabolic model, defining the ratio parameter as ratio in Equation (7), which serves as the dynamic correction benchmark; finally, converting the static sea level benchmark emission index (EI_0) to the dynamic EI value at the target altitude through a multi-parameter coupling formula. Take CO as an example. The emission index EI_{CO} of CO is shown in Equation (8).

$$\beta = e^{0.2 \times (M^2)} \tag{3}$$

$$\theta = \frac{T(alt)}{288.15\beta} \tag{4}$$

$$\delta = (1 - 0.0019812 \times alt) \times \frac{5}{288.15} \tag{5}$$

$$\omega = \frac{e^{-0.0001426*(alt-12900)}}{10^3} \tag{6}$$

$$ratio = FF_{actual}/FF_{ISA} \tag{7}$$

$$EI_{CO} = EI_{0,CO} \times ratio \tag{8}$$

In the formula, *M* is the Mach number. The ratio of the quasi-temperature (288.15K), FF is the fuel flow rate, and β, δ, ω, and ratio are the parameters for correcting *EI* under the ISA working condition. EI_0 is the emission index at sea level, and *EI* is the correction result. For common pollutants such as NO_x, CO, and HC, the emission index is calculated separately according to their specific correction formulas, ensuring that the emission calculations fully consider variations in emissions under different flight conditions. This leads to a more accurate estimation of pollutant emissions.

2.2. 3D space estimation

3D estimation is based on the trajectory points of aviation emissions at low altitudes and uses the 3D Empirical Bayesian Kriging method to construct a 3D aviation emissions voxel dataset(Gribov and Krivoruchko, 2020). Before using the 3D Empirical Bayesian Kriging method to expand the spatial data, the normal distribution of the interpolation data must first be tested. Only when the data follows a normal distribution can the Kriging method be used for interpolation. Descriptive statistical analysis of the samples is performed using SPSS 22.0. The K-S test is used to determine whether the data follows a normal distribution. For data that do not comply, a logarithmic transformation is applied to meet the normality criteria. After preprocessing, the 3D Empirical Bayesian Kriging method is used to construct the experimental area signal 3D spatial voxel dataset, and K-Bessel is selected for the transformation type to achieve 3D spatial expansion. The formula for the 3D Empirical Bayesian Kriging method is shown in Equation (9), where Z(u)

represents the interpolation at the target location u, n is the number of sampling points, Z_i is the observation value at the i-th sampling point, and λ_i (u) is the interpolation weight, representing the contribution of sampling point i to the target location u.

$$Z(u) = \sum_{i=1}^{n} \lambda_i(u) Z_i \qquad (9)$$

2.3. Emission hotspot identification

In the initial part of the algorithm, this study employs a voxel-by-voxel traversal method, using each voxel in the dataset as the center voxel to calculate the Local Emission Peak Indicator (LEPI). LEPI, as an indicator, signifies whether the aviation emissions in a local neighborhood are in a relatively high peak state, and its numerical value reflects the degree of relative high values. This study defines the concept of neighborhood: let the current center voxel be p, with coordinates (x, y, z), and establish a local coordinate system at the center voxel p, where the z-direction is the normal direction, and x and y are perpendicular to z. In this coordinate system, a cube with the center voxel p as its centroid and a side length of $2d_{cartesian}$ is created. The study determines that the

neighborhood voxel set N_p of voxel p is distributed at the 8 vertex voxels and the midpoint voxels on the 12 edges of the cube, as shown in Fig. 2. The center voxel p and the neighborhood voxel set N_p have a regular positional relationship in the 3D coordinate system: $\Delta d \in \{0, d_{cartesian}, -d_{cartesian}\}$. In this coordinate system, the coordinates of the center voxel p (x, y, z), and the neighborhood voxel set N_p can be expressed as:

$$N_p = \{(x + \Delta d, y + \Delta d, z + \Delta d)\} \\ \Delta d \in \{0, d_{cartesian}, -d_{cartesian}\} \qquad (10)$$

Based on the concept of neighborhood, the calculation formula for the LEPI is as follows:

$$K_i = [I(x_i, y_i, z_i) - I(x, y, z)]^2$$

$$LEPI_{(p_i)} = \frac{\sum_{i=1}^{\delta} K_i}{\delta} \qquad (11)$$

In the above formula, I (x, y, z) represents the signal intensity value at

the coordinates (x, y, z) of the center voxel, while $I(x_i, y_i, z_i)$ represents the value of the voxels in the neighborhood voxel set, with coordinates (x_i, y_i, z_i). K_i represents the local variance between the center voxel p and the neighborhood voxel set N_p, and δ represents the number of neighborhood voxels. Based on the above steps, the same calculation is performed for each voxel in the dataset, forming a set LEPIS = {LEPI (p_1), LEPI (p_2), …, LEPI (p_n)}.

The main criterion for High-emission discrimination is the threshold $d_{threshold}$. The purpose of threshold selection is to accurately determine the threshold through quantitative analysis. Setting the threshold is key to distinguishing between high-emission and normal voxels and must be based on the voxel variability calculated from the distribution characteristics of the dataset. Below is a method for selecting the threshold. The LEPIS sequence is then sorted in ascending order to form a sorted sequence $LEPIS_{sorted}$. A curve is fitted to the sorted $LEPIS_{sorted}$, where the vertical coordinate y represents LEPI, and the horizontal coordinate x represents the index p_i of the center voxel sorted by $LEPIS_{sorted}$. Since the distribution of p_i is equidistant, the first difference of the LEPI values should be calculated to approximate the slope $\Delta LEPI(p_i) = LEPI(p_{i+1}) - LEPI(p_i)$; the second difference $\Delta^2 LEPI(p_i)$ is then calculated to approximate the change in slope:

$$\Delta^2 LEPI(p_i) = \Delta LEPI(p_{i+1}) - \Delta LEPI(p_i) = \left(LEPI(p_{i+2}) - LEPI(p_{i+1}) - (LEPI(p_{i+1}) - LEPI(p_i)) \right) \qquad (12)$$

Then, traverse all the second differences $\Delta^2 LEPI(p_i)$ to find the voxel with the largest absolute value, which will be the threshold $d_{threshold}$. The selection of abnormal voxels is based on the determined threshold $d_{threshold}$. Voxels with LEPI greater than the threshold are selected from all voxels and are recognized as high-emission voxels, forming the set $\gamma_{peak} = \{p_i | LEPI(p_i) > d_{threshold}, p_i \in \gamma\}$. Where γ is the set of all the voxels. This paper uses the 3D DBSCAN algorithm to cluster γ_{peak} into 3D high emission irregular hotspots. The 3D DBSCAN algorithm is based on neighborhood parameter sets (Eps, MinPts) to quantify the internal compactness of the data sample voxel set. In the experiments, multiple neighborhood distance thresholds (Eps) were set for testing, with a default minimum sample size threshold (MinPts) of 10, used for noise and small region clustering to remove noise. The optimal clusters are selected as the research areas included in the study scope.
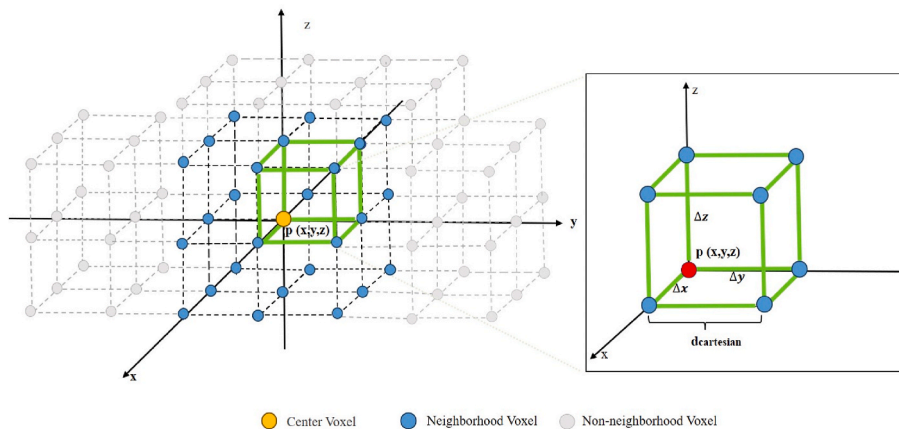

Fig. 2. The p voxel and its neighborhood voxel set.

3. Case study

3.1. Data

This paper selects Beijing Capital International Airport as the study area, using the trajectory points of aircraft from the ADS-B system and Flightradar24 for emission estimation and hotspot detection. The ADS-B system is widely used in aviation monitoring, allowing aircraft to automatically send flight-related information to ground stations, thereby enabling effective monitoring of aircraft status(Yang et al., 2023). The ADS-B trajectory data in this study comes from Flightradar 24, used to obtain trajectories during the actual flight operation phases of takeoff (LTO) and cruise descent (CCD). Each aircraft generates a position record every 30–45 s during flight via the Global Navigation Satellite System (GNSS), recording information such as ICAO code, real-time coordinates, timestamps, flight altitude, and ground speed. In addition, the flight schedule information (such as ICAO code, flight duration, departure and arrival airport codes, aircraft type, and engine manufacturer and number) is also sourced from Flightradar 24. The ICAO code is used to link ADS-B trajectory data with flight schedule data, creating a complete dataset for emissions calculation. Data samples can be found in Table 1, and the spatial distribution of some ADS-B waypoints is illustrated in Fig. 3. Table 1 displays the attributes of the ADS-B trajectory data, with each flight trajectory corresponding to a complete set of trajectory records.

3.2. Emission of flights

We used the TrajEmission method to simulate civil aviation pollutants based on actual flight paths and an improved aircraft performance model, and developed an airport aviation emissions(carbon dioxide (CO_2), carbon monoxide (CO), hydrocarbons (HC), and nitrogen oxides (NO_x)) dataset (Wang et al., 2024b; Sun et al., 2020; Sun et al., 2019). The data is detailed in Table 2. The data sample date for PEK airport is October 16, 2021, with a total of 2491 points. The east-west span is 116°34′-116°37′30″, and the north-south span is 40°2′3″ - 40°7′, covering the entire Capital Airport. Since the main emission period of the aircraft is the LTO (Landing and Takeoff) phase, we set the altitude of the study to 3000 ft(Cao et al., 2019).

We perform descriptive statistical analysis on the collected emission data from Beijing Capital International Airport (PEK). The data sources include airport operation records, flight takeoff and landing data, energy consumption records, and ground service activity records. Descriptive statistics include calculating the mean, median, standard deviation, etc., to depict the basic characteristics of emissions at the airport. Table 3 presents the emission data for Beijing Capital Airport on October 16, 2021. The sample size is 2491, covering four types of pollutants: carbon dioxide (CO_2), carbon monoxide (CO), hydrocarbons (HC), and nitrogen oxides (NO_x). The total emissions, average emissions, standard deviation, and median for each pollutant are listed. Among them, CO_2 has the highest emissions, with an average emission of 539535.76 g, whereas HC has the lowest average emissions at only 180.07 g. Table 4 further breaks down these emission data, categorizing them into four flight phases: approach, climb, idle, and takeoff. Each phase has its own

Table 1
Partial aircraft emissions data of PEK.

Altitude/ft	Longitude	Latitude	Flight phase	Origin	Destination
0	116.5944	40.07761	takeoff	PEK	CKG
300	116.5968	40.0773	climb	PEK	CKG
400	116.5958	40.0825	climb	PEK	NTG
400	116.5975	40.0732	climb	PEK	SHA
300	116.6142	40.0822	climb	PEK	SHA
734.4488	116.5851	40.07979	approach	CTU	PEK
397.8346	116.5856	40.07947	approach	CTU	PEK
61.22047	116.5861	40.07916	approach	CTU	PEK

sample size and the total and average emissions for the four pollutants. Notably, although the climb phase has the smallest sample size, it has the highest average emissions of NO_x, reaching 5884.21 g. In contrast, the idle phase shows significantly higher average emissions for CO and HC, at 5376.77 g and 554.99 g, respectively. The takeoff phase has the largest sample size, and its average emissions of NO_x are also the highest, at 4205.52 g.

3.3. 3D estimation of PEK

Using the 3D empirical Bayesian kriging method, spatial predictions were made for the aviation emission data from Beijing Capital International Airport (PEK), generating CO_2, CO, HC and NO_x 3D aviation voxel datasets, as shown in Fig. 4. Every voxel dataset contains a total of 296,660 voxels. The resolution is $50 \times 50 \times 50$ m. In order to evaluate the performance of the 3D empirical Bayesian kriging method, we used the cross-validation method. Cross-validation is a leave-one-out resampling method that removes a single input point and uses the remaining points to predict the value of that point, then compares the predicted value with the actual measured value. Table 5 shows the cross-validation results of four aviation emission gases (CO_2, CO, HC, NO_x) after interpolation using the 3D Empirical Bayesian Kriging method (3D-EBK). These results include Average CRPS, Inside 90 Percent Interval, Inside 95 Percent Interval, Root-Mean-Square, Root-Mean-Square Standardized and Average Standard Error.

3.4. High emission irregular hotspots

By measuring the emission in the 3D voxel dataset, we obtained the LEPI for each voxel. The sorted LEPI sequence is illustrated in Fig. 5, which shows the LEPI curve based on the 3D voxel data. According to the aforementioned threshold selection process, the threshold of LEPI series for aviation CO_2 emissions is 65682013534.12, the threshold of LEPI series for aviation CO emissions is 330020.16, the threshold of LEPI series for aviation HC emissions is 3802.10, and the threshold of LEPI series for aviation NO_x emissions is 710000.86.

The results of detecting high emission irregular hotspots (HEIH) at PEK Airport using 3D-HEE are shown in Fig. 6. In the identification of high emission hotspots for CO_2 emissions, a total of three irregular hotspots were identified, labeled as CO_2 HEIH1, CO_2 HEIH2, and CO_2 HEIH3. As seen in Fig. 6(a), the CO_2 HEIHs are primarily located near the ground. According to the 3D-HEE results shown in Fig. 7(a), CO_2 HEIH1 is located on the west side of Terminal 1, CO_2 HEIH2 is on both sides of the Capital Airport Line, and CO_2 HEIH3 is at the taxiway. These are all relatively flat ellipsoids; the height of CO_2 HEIH1 and CO_2 HEIH2 ranges from 0 to 37.18 m, and the height of HEIH3 ranges from 0 to 18.59 m, consistent with the diffusion pattern of CO_2. Fig. 6(b) and (c) show the detection results of high emission hotspots for CO and HC, respectively named CO HEIH1-2 and HC HEIH1-2, with height ranges of 0–37.18 m. From Fig. 7(b), CO HEIH1 is located at 40.06°N–40.08°N, 116.58°E−116.61°E, and CO HEIH2 is located at the start of the airport runway. As shown in the figure, CO HEIH1-2 and HC HEIH1-2 have similar geographical locations and shapes, which may be related to their similar generation mechanisms. The high emission hotspot detection results for NO_x emissions are shown in Fig. 6(c). A total of five NO_x high emission hotspots were detected, named NO_x HEIH1-5. Among them, NO_x HEIH1 has the highest elevation, ranging from 389.03 m to 889.04 m, while NO_x HEIH3 has a height range of 0–539.03 m. The remaining hotspots are located at ground level, with a maximum height of 456.17 m.

Fig. 8 shows the distribution of emissions for HEIH: carbon dioxide (CO_2), carbon monoxide (CO), hydrocarbons (HC), and nitrogen oxides (NO_x). Each histogram has the mass of the pollutant (in g) on the horizontal axis and the number of samples on the vertical axis. The emission range for carbon dioxide is from 250,000 g to 1,500,000 g, with most samples concentrated between 750,000 and 1,000,000 g, totaling 56
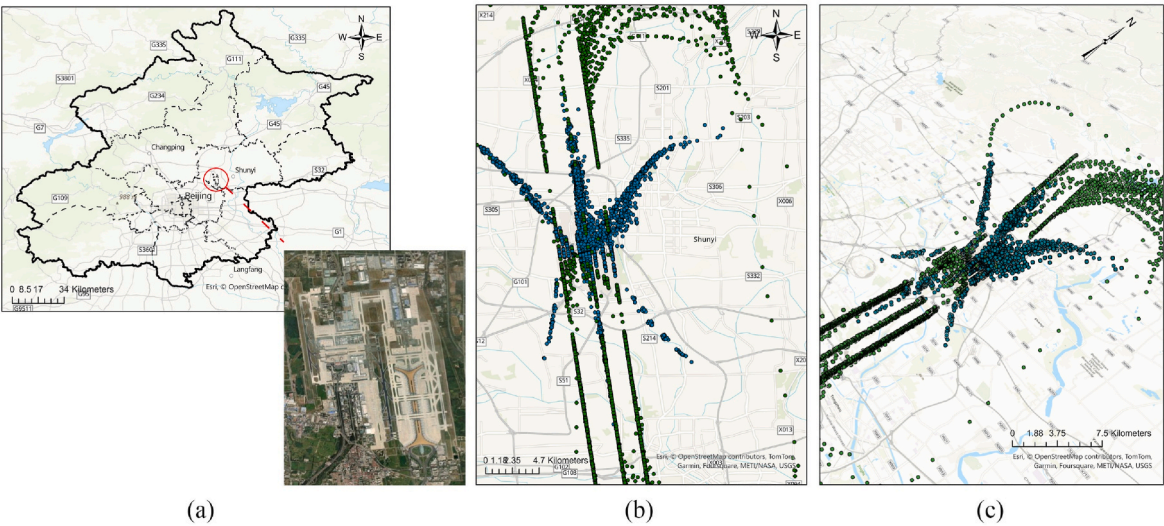
Fig. 3. The trajectory points of aviation emissions for PEK airport (Date: October 16, 2021). (a) The figure shows the geographical location of PEK airport; (b) The figure describes the two-dimensional distribution of trajectory points; (c) The figure describes the 3D distribution of trajectory points.

Table 2
Partial aircraft emissions data of PEK.

Altitude/ft	Longitude	Latitude	Flight phase	NO_x/g	CO/g	HC/g	CO_2/g	Origin	Destination
0	116.5944	40.07761	takeoff	888.4558	109.4157	7.566171	196431.6	PEK	CKG
300	116.5968	40.0773	climb	2845.168	230.4361	19.22742	526293.6	PEK	CKG
400	116.5958	40.0825	climb	3853.374	197.664	21.65063	618209.4	PEK	NTG
400	116.5975	40.0732	climb	10549.23	432.8389	10.25893	1567905	PEK	SHA
300	116.6142	40.0822	climb	7793.069	129.5378	0	753558.2	PEK	SHA
734.4488	116.5851	40.07979	approach	80.80055	449.004	26.50188	50908.8	CTU	PEK
397.8346	116.5856	40.07947	approach	80.08236	447.4945	26.42308	50780.77	CTU	PEK
61.22047	116.5861	40.07916	approach	79.34555	445.9696	26.3432	50651.09	CTU	PEK

Table 3
Descriptive statistics of emission data from PEK Airport.

Airport	Date	Sample Size	Emission	Total (g)	Average (g)	Standard Deviation (g)	Median (g)
PEK	20211016	2491	CO_2	1343444047.00	539535.76	478977.42	437007.32
PEK	20211016	2491	CO	4418403.14	1773.03	3139.76	408.66
PEK	20211016	2491	HC	448363.54	180.07	336.57	26.38
PEK	20211016	2491	NO_x	6868719.98	2758.52	3929.86	1123.44

Table 4
Emission data of different flight phase.

	Approach	Climb	Idle	Take off
Sample Size	507	184	723	1080
Total CO_2 (g)	78733026.58	157803647.25	584361602.66	522545770.31
Average CO_2 (g)	155598.86	862315.01	809365.11	484287.09
Total CO (g)	274085.78	47334.41	3882030.42	211404.08
Average CO (g)	541.67	258.65	5376.77	195.92
Total HC (g)	26879.49	2364.10	400704.52	18415.41
Average HC (g)	53.12	12.91	554.99	17.06
Total NO_x (g)	217812.13	1076812.11	1036332.02	4537763.70
Average NO_x (g)	430.45	5884.21	1435.36	4205.52

samples. The emission range for carbon monoxide varies from 0 g to 6000 g, peaking between 1000 and 1500 g, with nearly 280 samples. The emission range for hydrocarbons is from 0 g to 600 g, with a peak between 100 and 150 g and approximately 320 samples. Nitrogen oxides have the widest emission range, from 0 g to 9000 g, with a peak between 1500 and 4000 g and about 210 samples.

CO_2 HEIH1, CO_2 HEIH2, CO HEIH2, HC HEIH2, NO_x HEIH1, NO_x HEIH2, and NO_x HEIH3 correspond to the aircraft takeoff phase. These spatial hotspots directly correlate with peak fuel combustion rates during thrust generation. Jet fuel (primarily composed of hydrocarbons) produces CO_2, CO, NO_x, and HC when the C and N elements combine with oxygen during combustion. Consequently, as fuel consumption increases sharply, the emissions will correspondingly rise(Kerrebrock, 1992). Aerodynamic configurations during takeoff dominate emission spatial patterns. The aircraft must maintain a certain angle of attack to obtain sufficient lift, altering the distribution and magnitude of aerodynamic drag. During the takeoff roll, the deployment of landing gear, flaps, and changes in the fuselage-airflow angle result in significant increases in both parasitic and induced drag(Nicolosi et al., 2016; Chambers and Grafton, 1977; Kopecki and Rogalski, 2014). Maximum takeoff weight critically amplifies emission intensity. A fully loaded
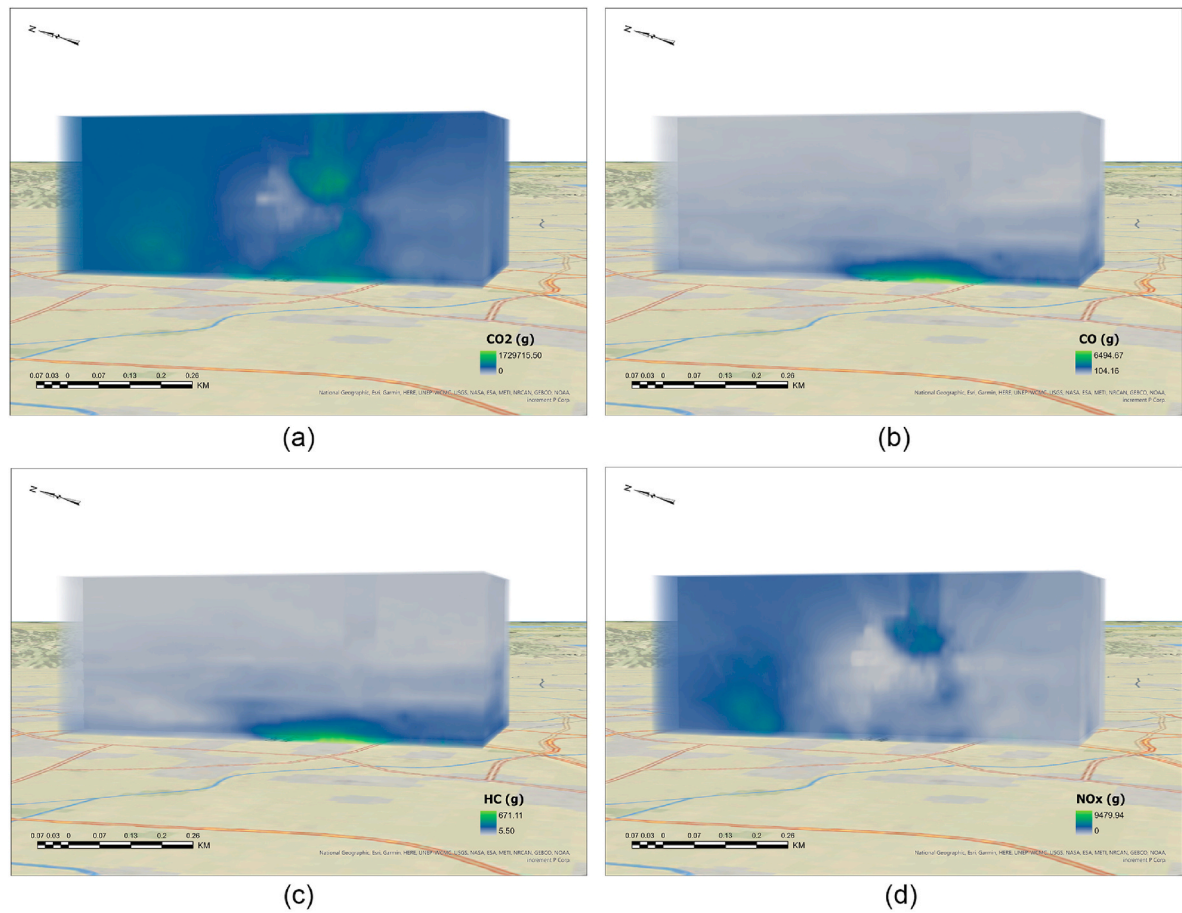
Fig. 4. 3D voxel data for PEK. (a) Visualization of voxel data on aviation CO_2 emissions; (b) Visualization of voxel data on aviation CO emissions; (c) Visualization of voxel data on aviation HC emissions; (d) Visualization of voxel data on aviation NO_x emissions.

Table 5
The cross-validation results of 3D-EBK interpolation for different aviation emissions data.

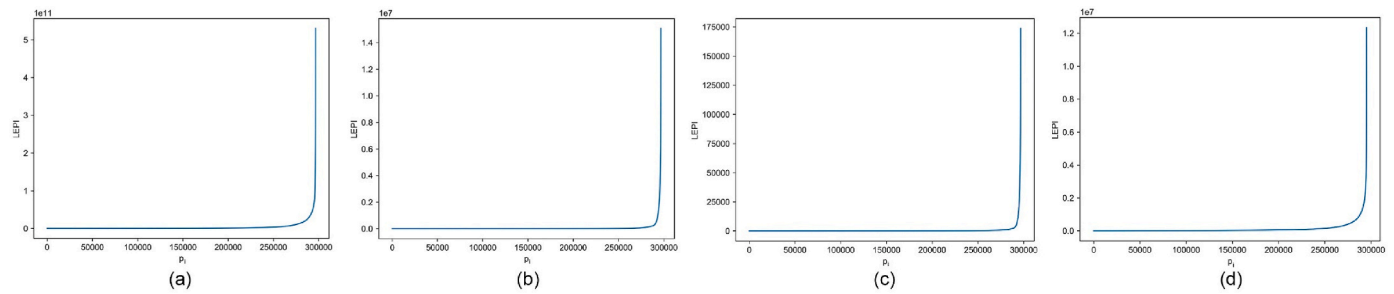| Data	Average CRPS	Inside 90 Percent Interval	Inside 95 Percent Interval	Root-Mean-Square	Root-Mean-Square Standardized	Average Standard Error
CO2	148110.75	91.29 %	94.78 %	290512.09	0.9827	288482.20
CO	354.91	94.41 %	96.61 %	987.13	0.8906	1021.31
HC	39.12	94.50 %	96.52 %	111.20	0.8552	113.52
NOx	896.60	93.31 %	95.42 %	1982.88	0.9178	2085.78

Fig. 5. LEPI distribution data for PEK. (a) LEPI series for aviation CO_2 emissions; (b) LEPI series for aviation CO emissions; (c) LEPI series for aviation HC emissions; (d) LEPI series for aviation NO_x emissions.

Boeing 777-300 ER (approximately 350 tons (Jakovljević et al., 2018)) requires engines to generate 90–110 % rated thrust during acceleration phases, directly linking weight parameters to emission magnitudes through fuel consumption dynamics. CO_2 HEIH3, CO HEIH1, HC HEIH1, NO_x HEIH4, and NO_x HEIH5 are associated with the approach and idle

phases. Lower combustion efficiency (58–72 % compared to 85–93 % at cruise thrust) in these phases elevates unit emission factors. Despite the LTO phase accounting for only 6–12 % of total flight duration in typical missions(Akdeniz, 2022; Balli, 2022; Aygun and Caliskan, 2021), emissions are concentrated near ground-level airspace. Proximity to
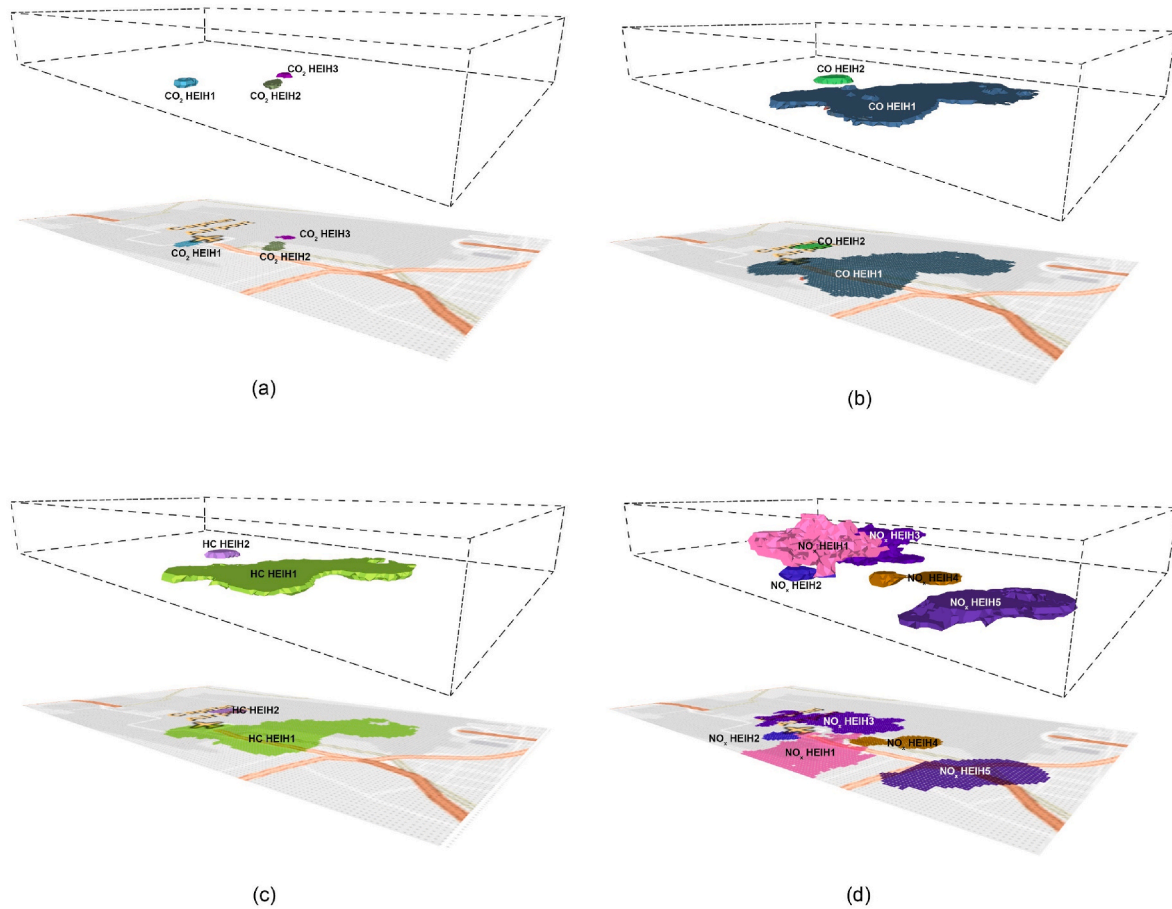
Fig. 6. Results of detecting High emission irregular hotspots (HEIH) at PEK. The dashed box in the figure represents the voxel dataset of aviation emissions, and the three-dimensional model inside it depicts the detected HEIH, with its position in the box corresponding to its position in the voxel data. The map at the bottom shows the two-dimensional projection of HEIH on the map. (a) shows the detection results for CO_2; (b) shows the detection results for CO; (c) shows the detection results for HC; (d) shows the detection results for NO_x.
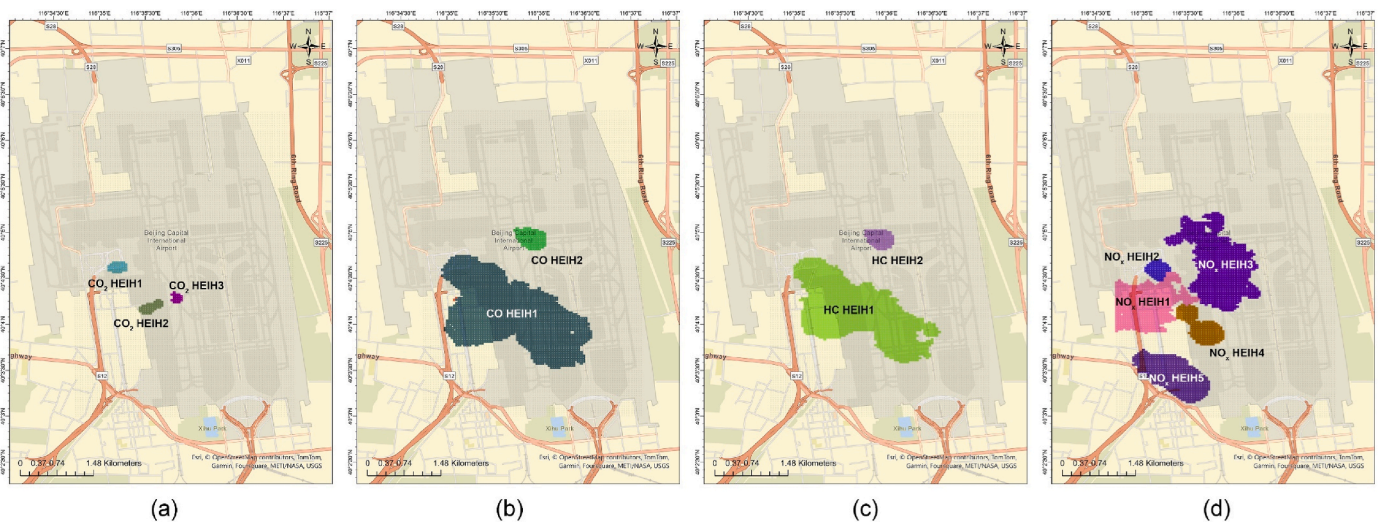

Fig. 7. 2D visualization of the HEIHs.

ground monitoring stations (≤300 m altitude) results in 3.2–5.1 times higher local pollutant impacts compared to high-altitude emissions (Testa et al., 2013).

4. Discussion

HEIHs are in the runway and taxiway areas, as well as the surrounding airport region (beyond the extended runway centerline, near the airport boundary, etc.), high emission from aircraft can have
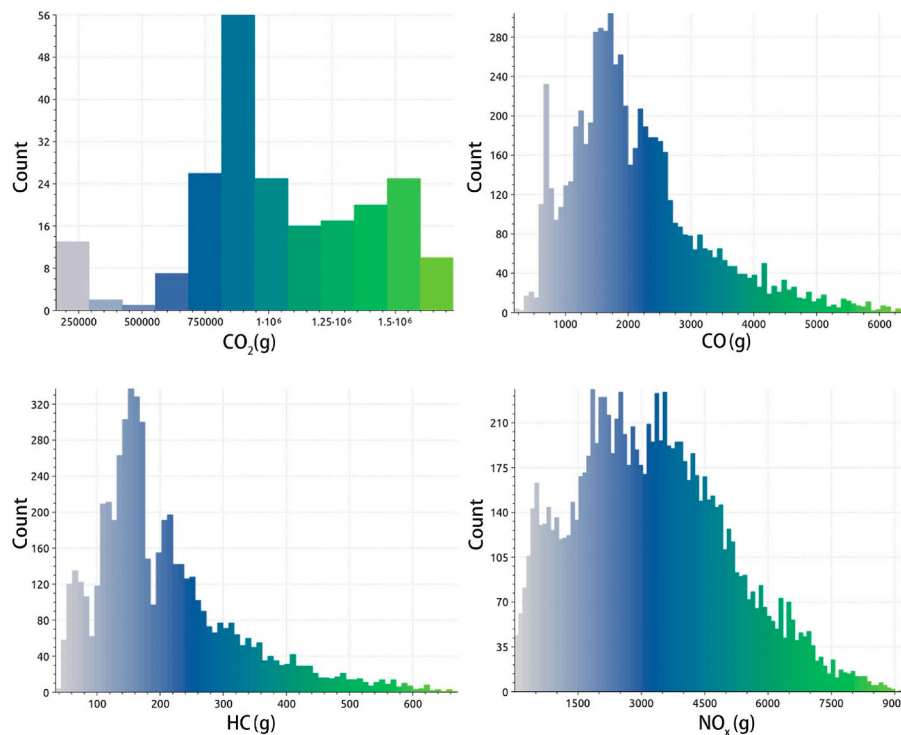
Fig. 8. The statistics of the data from all HEIHs. In all figures, the color indicates the emission content of the voxel.

multiple effects(Hu et al., 2022; Zhu et al., 2021). From an air quality perspective, this can lead to a sharp increase in local CO_2 CO HC and NO_x concentrations, affecting the health of airport ground staff, nearby residents, and organisms within the ecosystem. For example, runway personnel and nearby residents exposed to high concentrations of CO_2 and CO over a long period may experience respiratory discomfort, headaches, and other symptoms, while the balance of photosynthesis and respiration may also be disrupted for surrounding vegetation. In terms of meteorological conditions, CO_2, as a greenhouse gas, can interfere with the microclimate around runways and taxiways due to its abnormal increase, impacting the accuracy of meteorological monitoring data and posing potential risks to flight takeoff and landing decisions. Furthermore, high concentrations of emission gas may adversely affect precision equipment near the runways and taxiways, such as degrading the performance of runway visibility monitoring optical devices, leading to data deviations that affect pilots' judgments of runway conditions. In the surrounding airport area, the increased load of greenhouse gases due to abnormal emissions can trigger a series of environmental issues and may also raise concerns and worries among nearby residents regarding the environmental impact of the airport, potentially leading to social conflicts (Jensen et al., 2023).

From the perspective of engine operation and performance, aircraft takeoff requires the engine to produce tremendous thrust to quickly achieve the required takeoff speed within a limited runway length. During the takeoff phase, the engines typically operate at or near their maximum rated power. Modern jet engines significantly increase fuel flow during takeoff conditions to meet high thrust demands. This is because, according to the engine thrust formula, thrust is related to mass airflow and exhaust velocity increments. To generate sufficient thrust for acceleration, the engine must intake a large amount of air and eject high-speed exhaust gases, which consumes a significant amount of fuel (Kerrebrock, 1992). Regarding the high emission issues during the takeoff phase, we can implement a series of refined and explanatory energy-saving and emission reduction measures to provide precise decision support. First, by optimizing the engine combustion system, including new technologies such as the EGR system, twin-scroll

turbochargers, and 350-bar injection systems, we can improve engine efficiency, reduce fuel consumption, and decrease gas emissions(Cui and Chen, 2024; Wei et al., 2024; Martinez-Valencia et al., 2023). At the same time, the application of in-cylinder water injection technology can lower exhaust temperatures, suppress knocking, enhance ignition efficiency, and further reduce fuel consumption(Zhang et al., 2024). Furthermore, reducing internal engine friction is also an important direction for improving efficiency; although specific technical details are not elaborated, this is a technological area worthy of attention(Liu et al., 2024). In terms of operational management, optimizing operational area settings through market data analysis can enhance service efficiency and user experience. Strengthening energy-saving and emission reduction operational training for ground personnel can improve airport operational efficiency. Promoting the use of Sustainable Aviation Fuel (SAF) can reduce dependence on fossil fuels and significantly lower exhaust emissions(Uy and San Juan, 2024). Implementing key energy-saving and emission reduction projects while promoting energy-saving technologies and ultra-low emission transformations can improve the energy efficiency benchmarks of the industry. Strengthening the construction and application of an online energy consumption monitoring system, perfecting the energy consumption statistics system and indicator system, will help build a fixed pollution source monitoring system.

In idle mode, the aircraft engine still consumes fuel to keep running; although the fuel consumption rate is relatively low at this point, the fuel emissions per unit of fuel may increase due to reduced combustion efficiency. Emissions from the aircraft in the approach and idle states are directly released into the air near the airport, and due to the lower flight altitude, these emissions have a more direct and significant impact on the surrounding environment and air quality (Liu et al., 2020; Jonsdottir et al., 2019; Masiol and Harrison, 2014b). In response to the high emission issues during the approach and idle phases, comprehensive measures can be taken to promote the sustainable development of the airport aviation industry and reduce emissions. First, by optimizing the procedures for aircraft approach and idle operations, unnecessary fuel consumption can be reduced, for example, by adopting more precise approach paths and speed control (Rodríguez-et al., 2019). Second,

improving ground operation efficiency, such as using ground power and air conditioning systems instead of the aircraft's Auxiliary Power Unit (APU) while the aircraft waits for takeoff and landing, can reduce fuel consumption and emissions during idling(Fernandes et al., 2018). At the same time, promoting the use of sustainable aviation fuels (such as biofuels), which produce lower carbon emissions during combustion, can help reduce the overall carbon footprint (Cui and Chen, 2024). Additionally, improving engine combustion efficiency, especially during low-load operations, can reduce HC and CO emissions caused by incomplete combustion, thereby indirectly reducing CO_2 emissions (Ng et al., 2021). Installing emission reduction facilities near airports, such as ground emission capture systems, can reduce the pollutants released into the air during aircraft idling and approach phases. Optimizing airport ground traffic can reduce the time and distance aircraft spend taxiing on the ground, thus decreasing fuel consumption and emissions during idling and taxiing phases(Monsalud et al., 2015; Polishchuk et al., 2019).

This study successfully applied the 3D-HEE method to PEK, revealing the HEIHs within the airport in more detail. Several key findings emerged from the experiments: First, although the regular voxel structure presented irregular shapes in some areas with missing values, the algorithm focused solely on the local emission differences between voxels without considering spatial relationships, yet still achieved good extraction results. Second, the method successfully utilized 3D DBSCAN to extract 3D structures, effectively filtering out scattered noise voxels caused by errors in the original data. In terms of visualization, this algorithm allows for the observation of spatial variations in airport aviation emissions from multiple dimensions, presenting the extracted HEIH structures intuitively. This not only helps deepen the understanding of HEIH characteristics but also provides researchers with a more intuitive tool to interpret and communicate their findings.

However, it is important to note that the dataset used consists of regenerated data from aircraft trajectories, and the location attributes must be representative. Although the study achieved results consistent with the distribution of airport aircraft status and was validated through causal analysis, this does not guarantee that detection accuracy is absolutely precise. Future work should consider using datasets with higher confidence and explore the impact of interpolation methods on the extraction accuracy of the algorithms.

5. Conclusion

This study proposed a 3D High Emission Estimation method (3D-HEE) to construct high-dimensional emissions of airport and detect its irregular 3D hotspot. This method combines Emission estimation, 3D space estimation, and Emission hotspot identification. We employ 3D-HEE method for 3D HEIH detection at Beijing Capital International Airport (PEK). Successfully identifying high emission irregular hotspots such as CO_2, CO, HC and NO_x HEIHs, thus confirming its effectiveness in airport emission research. The results show that the high thrust operation of the engine, the change of combustion efficiency, the take-off attitude and weight of the aircraft lead to HEIHs during the take-off phase. During the aircraft's approach and idle phases, the low engine load results in incomplete fuel combustion, leading to HEIHs. This study provides empirical support for energy-saving and emission-reduction measures at airports, aiding in the formulation of targeted strategies, which are significant for achieving carbon peak and carbon neutrality goals and global climate action. However, airport aviation emission management still faces numerous challenges that require further in-depth research and improvement.

CRediT authorship contribution statement

Zhoushun Han: Writing – review & editing, Writing – original draft, Visualization, Software, Resources, Methodology, Data curation, Conceptualization. **Hengcai Zhang:** Writing – review & editing,

Supervision, Software, Resources, Project administration, Methodology, Conceptualization. **Jinzi Wang:** Visualization, Validation, Software, Methodology, Conceptualization. **Xin Fu:** Writing – review & editing, Methodology, Data curation. **Peixiao Wang:** Supervision, Methodology, Conceptualization. **Jianing Yu:** Supervision, Methodology. **Yafei Li:** Resources.

Declaration of competing interest

The authors declare that they have no known competing financial interests or personal relationships that could have appeared to influence the work reported in this paper.

Data availability

Data will be made available on request.

References

Akdeniz, H.Y., 2022. Landing and take-off (LTO) flight phase performances of various piston-prop aviation engines in terms of energy, exergy, irreversibility, aviation, sustainability and environmental viewpoints. Energy 243, 123179.

Ashok, A., 2011. The Air Quality Impact of Aviation in future-year Emissions Scenarios.

Ashok, A., Balakrishnan, H., Barrett, S.R., 2017. Reducing the air quality and CO2 climate impacts of taxi and takeoff operations at airports. Transport. Res. Transport Environ. 54, 287–303.

Aygun, H., Caliskan, H., 2021. Environmental and enviroeconomic analyses of two different turbofan engine families considering landing and take-off (LTO) cycle and global warming potential (GWP) approach. Energy Convers. Manag. 248, 114797.

Balli, O., 2022. Thermodynamic, thermoenvironmental and thermoeconomic analyses of piston-prop engines (PPEs) for landing and take-off (LTO) flight phases. Energy 250, 123725.

Bastress, E.K., 1973. Impact of aircraft exhaust emissions at airports. Environ. Sci. Technol. 7 (9), 811–816.

Cao, H., Miao, J., Miao, L., Tang, X., 2019. Research on estimation method of daily emission inventory of aircraft engine in beijing capitalinternationalairport based on real flight data. Acta Sci. Circumstantiae 39 (8), 2699–2707.

Chambers, J.R., Grafton, S.B., 1977. Aerodynamic Characteristics of Airplanes at High Angles of Attack.

Chen, H., Liang, M., Liu, W., Wang, W., Liu, P.X., 2022. An approach to boundary detection for 3D point clouds based on DBSCAN clustering. Pattern Recogn. 124, 108431.

Christodoulakis, J., Karinou, F., Kelemen, M., Kouremadas, G., Fotaki, E.F., Varotsos, C. A., 2022. Assessment of air pollution from Athens international airport and suggestions for adaptation to new aviation emissions restrictions. Atmos. Pollut. Res. 13 (6), 101441. https://doi.org/10.1016/j.apr.2022.101441.

Cui, Q., Chen, B., 2024. Cost-benefit analysis of using sustainable aviation fuels in South America. J. Clean. Prod. 435, 140556. https://doi.org/10.1016/j.jclepro.2024.140556.

Du, K., Xie, C., Ouyang, X., 2017. A comparison of carbon dioxide (CO2) emission trends among provinces in China. Renew. Sustain. Energy Rev. 73, 19–25.

Fernandes, M.D., et al., 2018. SOFC-APU systems for aircraft: a review. Int. J. Hydrogen Energy 43 (33), 16311–16333.

Fung, M.K.Y., Wan, K.K.H., Van Hui, Y., Law, J.S., 2008. Productivity changes in Chinese airports 1995–2004. Transport. Res. E Logist. Transport. Rev. 44 (3), 521–542.

Graham, W.R., Hall, C.A., Morales, M.V., 2014. The potential of future aircraft technology for noise and pollutant emissions reduction. Transp. Policy 34, 36–51.

Graver, B.M., Frey, H.C., 2009. Estimation of air carrier emissions at Raleigh-Durham international airport. In: Proceedings, 102nd Annual Conference and Exhibition, Air and Waste Management Association. Citeseer.

Gribov, A., Krivoruchko, K., 2020. Empirical bayesian kriging implementation and usage. Sci. Total Environ. 722, 137290.

Hu, R., Zhu, J., Zhang, Y., Zhang, J., Witlox, F., 2020. Spatial characteristics of aircraft CO2 emissions at different airports: some evidence from China. Transport. Res. Transport Environ. 85, 102435.

Hu, Y.-J., Yang, L., Cui, H., Wang, H., Li, C., Tang, B.-J., 2022. Strategies to mitigate carbon emissions for sustainable aviation: a critical review from a life-cycle perspective. Sustain. Prod. Consum. 33, 788–808.

Jakovljević, I., Mijailović, R., Mirosavljević, P., 2018. Carbon dioxide emission during the life cycle of turbofan aircraft. Energy 148, 866–875.

Jensen, L.L., Bonnefoy, P.A., Hileman, J.I., Fitzgerald, J.T., 2023. The carbon dioxide challenge facing US aviation and paths to achieve net zero emissions by 2050. Prog. Aero. Sci. 141, 100921.

Jonsdottir, H.R., et al., 2019. Non-volatile particle emissions from aircraft turbine engines at ground-idle induce oxidative stress in bronchial cells. Commun. Biol. 2 (1), 90.

Kelemen, M., et al., 2020. Educational model for evaluation of airport NIS security for safe and sustainable air transport. Sustainability 12 (16), 6352. https://doi.org/10.3390/su12166352.

Kerrebrock, J.L., 1992. Aircraft Engines and Gas Turbines. MIT press.

Kılkış, B., 2014. Energy consumption and CO2 emission responsibilities of terminal buildings: a case study for the future istanbul international airport. Energy Build. 76, 109–118.

Klapmeyer, M.E., Marr, L.C., 2012. CO2, NO X, and particle emissions from aircraft and support activities at a regional airport. Environ. Sci. Technol. 46 (20), 10974–10981.

Kopecki, G., Rogalski, T., 2014. Aircraft attitude calculation with the use of aerodynamic flight data as correction signals. Aero. Sci. Technol. 32 (1), 267–273.

Lee, D.S., et al., 2009. Transport impacts on atmosphere and climate: aviation. Atmos. Environ. 44, 4678–4734.

Liu, X., Hang, Y., Wang, Q., Zhou, D., 2020. Drivers of civil aviation carbon emission change: a two-stage efficiency-oriented decomposition approach. Transport. Res. Transport Environ. 89, 102612.

Liu, H., Yu, S., Wang, T., Li, J., Wang, Y., 2024. A systematic review on sustainability assessment of internal combustion engines. J. Clean. Prod. 451, 141996. https://doi.org/10.1016/j.jclepro.2024.141996.

Mackenzie, D., 2010. ICAO: a History of the International Civil Aviation Organization. University of Toronto Press.

Mardani, A., Streimikiene, D., Cavallaro, F., Loganathan, N., Khoshnoudi, M., 2019. Carbon dioxide (CO2) emissions and economic growth: a systematic review of two decades of research from 1995 to 2017. Sci. Total Environ. 649, 31–49.

Martinez-Valencia, L., Peterson, S., Brandt, K., King, A.B., Garcia-Perez, M., Wolcott, M., 2023. Impact of services on the supply chain configuration of sustainable aviation fuel: the case of CO2e emission reductions in the U.S. J. Clean. Prod. 404, 136934. https://doi.org/10.1016/j.jclepro.2023.136934.

Masiol, M., Harrison, R.M., 2014a. Aircraft engine exhaust emissions and other airport-related contributions to ambient air pollution: a review. Atmos. Environ. 95, 409–455.

Masiol, M., Harrison, R.M., 2014b. Aircraft engine exhaust emissions and other airport-related contributions to ambient air pollution: a review. Atmos. Environ. 95, 409–455.

Monsalud, A., Ho, D., Rakas, J., 2015. Greenhouse gas emissions mitigation strategies within the airport sustainability evaluation process. Sustain. Cities Soc. 14, 414–424.

Ng, K.S., Farooq, D., Yang, A., 2021. Global biorenewable development strategies for sustainable aviation fuel production. Renew. Sustain. Energy Rev. 150, 111502.

Nicolosi, F., Corcione, S., Della Vecchia, P., 2016. Commuter aircraft aerodynamic characteristics through wind tunnel tests. Aircraft Eng. Aero. Technol.: Int. J. 88 (4), 523–534.

Ouyang, X., Lin, B., 2017. Carbon dioxide (CO2) emissions during urbanization: a comparative study between China and Japan. J. Clean. Prod. 143, 356–368.

Polishchuk, V., et al., 2019. A fuzzy model of risk assessment for environmental Start-Up projects in the air transport sector. Int. J. Environ. Res. Publ. Health 16 (19), 3573. https://doi.org/10.3390/ijerph16193573.

Rodríguez-Díaz, A., Adenso-Díaz, B., González-Torre, P.L., 2019. Improving aircraft approach operations taking into account noise and fuel consumption. J. Air Transport. Manag. 77, 46–56.

Sun, J., Ellerbroek, J., Hoekstra, J.M., 2019. WRAP: an open-source kinematic aircraft performance model. Transport. Res. C Emerg. Technol. 98, 118–138. https://doi.org/10.1016/j.trc.2018.11.009.

Sun, J., Hoekstra, J.M., Ellerbroek, J., 2020. OpenAP: an open-source aircraft performance model for air transportation studies and simulations. Aerospace 7 (8), 104.

Sun, J., et al., 2022. OpenSky report 2022: evaluating aviation emissions using crowdsourced open flight data. In: 2022 IEEE/AIAA 41st Digital Avionics Systems Conference (DASC), pp. 1–8.

Takeda, K., Takeda, A., Bryant, J., Clegg, A., 2008. Systematic review of the impact of emissions from aviation on current and future climate. Aeronaut. J. 112, 493–522, 1968.

Testa, E., Giammusso, C., Bruno, M., Maggiore, P., 2013. Fluid dynamic analysis of pollutants' dispersion behind an aircraft engine during idling. Air Qual. Atmos. Health 6, 367–383.

Uy, J.G., San Juan, J.L., 2024. Multi-objective optimization of airline fuel loading problem considering sustainable aviation fuel and book-and-claim. J. Clean. Prod. 482, 144241. https://doi.org/10.1016/j.jclepro.2024.144241.

Varotsos, C.A., Krapivin, V.F., Soldatov, V.Y., 2014. Modeling the carbon and nitrogen cycles. Front. Environ. Sci. Rev. ume 2. https://doi.org/10.3389/fenvs.2014.00008 (in English).

Wang, Y.-n., et al., 2023. Emissions from international airport and its impact on air quality: a case study of beijing daxing international airport (PKX), China. Environ. Pollut. 336, 122472.

Wang, J., Zhang, H., Yu, J., Lu, F., Li, Y., 2024a. Modeling civil aviation emissions with actual flight trajectories and enhanced aircraft performance model. Atmosphere 15 (10), 1251 [Online]. Available: https://www.mdpi.com/2073-4433/15/10/1251.

Wang, J., Zhang, H., Yu, J., Lu, F., Li, Y., 2024b. Modeling civil aviation emissions with actual flight trajectories and enhanced aircraft performance model. Atmosphere 15 (10). https://doi.org/10.3390/atmos15101251.

Wei, S., Li, Y., Wu, L., Zhang, Z., Yan, S., Ran, W., 2024. Combustion chemical reaction mechanism and kinetic analysis of RP-3 aviation kerosene/low carbon alcohol blends. J. Clean. Prod. 469, 143202. https://doi.org/10.1016/j.jclepro.2024.143202, 2024/09/01/.

Xiong, X., Song, X., Kaygorodova, A., Ding, X., Guo, L., Huang, J., 2023. Aviation and carbon emissions: evidence from airport operations. J. Air Transport. Manag. 109, 102383. https://doi.org/10.1016/j.jairtraman.2023.102383, 2023/06/01/.

Yang, Z., Kang, X., Gong, Y., Wang, J., 2023. Aircraft trajectory prediction and aviation safety in ADS-B failure conditions based on neural network. Sci. Rep. 13 (1), 19677. https://doi.org/10.1038/s41598-023-46914-2.

Yaohui, L., Jinglei, Y., Juan, G., Wenjun, S., Xiaolin, J., Yu, H., 2023. Review of research on CO 2 emissions from civil aviation flights and its impact on climate change. Adv. Earth Sci. 38 (1), 9.

Yildiz, O.F., Yilmaz, M., Celik, A., 2022. Reduction of energy consumption and CO2 emissions of HVAC system in airport terminal buildings. Build. Environ. 208, 108632. https://doi.org/10.1016/j.buildenv.2021.108632.

Zhang, W., et al., 2019. Effects of urbanization on airport CO2 emissions: a geographically weighted approach using nighttime light data in China. Resour. Conserv. Recycl. 150, 104454.

Zhang, J., Kong, L., Yang, B., Xu, B., 2024. Clean and sustainable recovery of valuable materials from InP scrap via controlled-pressure pyrolysis–spray condensation. J. Clean. Prod. 475, 143613. https://doi.org/10.1016/j.jclepro.2024.143613.

Zhu, C., Hu, R., Liu, B., Zhang, J., 2021. Uncertainty and its driving factors of airport aircraft pollutant emissions assessment. Transport. Res. Transport Environ. 94, 102791.